Fertilization-driven Pulses of Atmospheric Nitrogen Dioxide Complicate Air Pollution in Early Spring over the North China Plain

Tian Feng,[1] Guohui Li,[2,*] Shuyu Zhao,[3] Naifang Bei,[4] Xin Long,[5] Yuepeng Pan,[6] Yu Song,[7] Ruonan Wang,[2] Xuexi Tie,[2] Luisa T. Molina[8]

[1] Department of Geography & Spatial Information Techniques, Ningbo University, Ningbo, China
[2] KLACP, State Key Laboratory of Loess and Quaternary Geology, Institute of Earth Environment, Chinese Academy of Sciences, Xi'an, China
[3] Ningbo Meteorological Bureau, Ningbo, China
[4] School of Human Settlements and Civil Engineering, Xi'an Jiaotong University, Xi'an, China
[5] Research Center for Atmospheric Environment, Chongqing Institute of Green and Intelligent Technology, Chinese Academy of Sciences, Chongqing, China
[6] State Key Laboratory of Atmospheric Boundary Layer Physics and Atmospheric Chemistry (LAPC), Institute of Atmospheric Physics, Chinese Academy of Sciences, Beijing, China
[7] State Key Joint Laboratory of Environmental Simulation and Pollution Control, Department of Environmental Science, Peking University, Beijing, China
[8] Molina Center for Energy and the Environment, Boston, MA, USA

*Corresponding author. Email: ligh@ieecas.cn

Abstract

Atmospheric nitrogen dioxide (NO_2) has shown periodic conspicuous pulses in tropospheric column in March over the North China Plain during the past two decades. However, these repetitive pulses have never been reported and its underlying causes remain unclear. Here, we present robust evidence to demonstrate that agricultural fertilization drives the early-spring NO_2 column increases. The fertilization-driven soil NO_x (=NO+NO_2) emissions, comparable to anthropogenic sources, exert complicated influences on regional air quality. They significantly reduce nocturnal and diurnal O_3 concentrations in agricultural areas in early spring, distinct from the scenarios in summer, but increase fine particulate matter ($PM_{2.5}$) concentrations via strongly enhancing nitrate aerosol formation. The impact also extends to urban areas, approximately half that of agricultural areas. These findings are with increasing implications for coordinated control of $PM_{2.5}$ and O_3 under global warming. We thus suggest that reducing NO_x emissions in croplands is essential to achieve better air quality in agricultural countries and regions.

Short Summary

Impacts of agricultural fertilization on nitrogen oxide and air quality are becoming more pronounced with continuous reductions in fossil fuel sources in China. We report that atmospheric nitrogen dioxide pulses driven by agricultural fertilizations largely complicate air pollution in the North China Plain, highlighting the necessity of agricultural emission control.

Keywords: Nitrogen Dioxide, Fertilization, Air Pollution, Ozone, $PM_{2.5}$

1 Introduction

Nitrogen oxide (NO_x = nitric oxide (NO) + nitrogen dioxide (NO_2)) is a major air pollutant in the troposphere and a key precursor to ozone (O_3) and fine particulate matter ($PM_{2.5}$) due to its photochemical properties (Seinfeld and Pandis, 2006; Zhang et al., 2015). It is also a short-lived climate forcer regulated by both China and the United States (IPCC, 2023). Understanding the NO_x budget is crucial for addressing these issues. Globally, atmospheric NO_x is mainly produced by fossil fuel combustion (Crippa et al., 2023; Janssens-Maenhout et al., 2015; Yan et al., 2005), with smaller contributions from wildfires and lightning (Bauwens et al., 2020; Murray et al., 2012). Additionally, soil generates substantial NO_x through nitrification and denitrification processes (Bouwman et al., 2002; Cárdenas et al., 1993; Davidson, 1992; Yan et al., 2005), particularly after the rewetting of dry soils (Galbally and Roy, 1978; Huber et al., 2020; Yienger and Levy, 1995). On a regional scale, soil NO_x emissions maybe even exceed those from fossil fuel sources in summer (Almaraz et al., 2018; Sha et al., 2021). Model- and satellite-based studies estimate that global annual soil NO emissions, with the largest contributor of cultivated croplands, range from 9 to 27 Tg N (Hudman et al., 2012; Steinkamp and Lawrence, 2011; Vinken et al., 2014; Yan et al., 2005), accounting for about 15% of total NO_x emissions (Hudman et al., 2012). This wide range is due to the complex response of soil NO_x emissions to driving factors like fertilization, temperature, and soil moisture (Huber et al., 2020; Oikawa et al., 2015), making accurate estimation challenging.

The emission rates from fertilized croplands are 1 to 2 orders of magnitude higher than nearby grasslands and forest soils (Almaraz et al., 2018; Anderson and Levine, 1987; Guo et al., 2020; Yienger and Levy, 1995). Recent studies show significant NO_x emissions from croplands post-fertilization, exceeding pre-fertilization rates by an order of magnitude (Almaraz et al., 2018; Hickman et al., 2017; Laville et al., 2011; Liu et al., 2005; Oikawa et al.,

2015; Zhao et al., 2015). Despite these robust evidences of strong NO_x emissions from agricultural fertilization, the lack of extensive *in-situ* measurements hinders accurate estimation of these emissions and their environmental impacts. Additionally, the effect of agricultural fertilization on air quality has not received sufficient global attention, although some pioneering studies have pointed the implications for air quality since the 1990s (Davidson et al., 1998; Hall et al., 1996). In recent years, studies have reported that agricultural soil emissions significantly increase atmospheric NO_x levels (Almaraz et al., 2018; Hickman et al., 2017; Huang et al., 2018; Oikawa et al., 2015) and enhance O_3 formation in summer in California (Oikawa et al., 2015) or during the growing season of crops in sub-Saharan Africa (Hickman et al., 2017; Huang et al., 2018).

The North China Plain (NCP) is one of the major grain-producing regions in China. Winter wheat-maize double cropping is a typical rotation system mainly practiced in this region (Liu et al., 2003; Zhu et al., 1994). China has been the world's largest consumer of N-fertilizer since 2000 (Liu et al., 2013), with annual usage peaking at approximately 31.2 Tg N in 2014 (Yu et al., 2022). About half of this fertilizer is lost to the environment (Liu et al., 2013), indicating a significant potential source for NO_x emissions from China's croplands. The agricultural management in the NCP has been known for incorporating high fertilization rates with excessive N fertilization (Sun et al., 2022; Vitousek et al., 2009; Zhao et al., 2006). Thus, this region is the largest consumer of agricultural fertilizer N in China (Yu et al., 2022) and has shown substantial soil NO_x emissions (Liu et al., 2010; Tang et al., 2020; Zhang et al., 2011). The emissions significantly increase ambient NO_x levels and enhance O_3 formation in summer (Huang et al., 2023; Lu et al., 2021; Wang et al., 2022a). These concerns typically focus on the warm season when higher temperatures favor NO_x emissions from soils. However, frequent agricultural activities and N-fertilizer use also occur during transitional seasons, and how

93 periodic agricultural fertilization affects soil NO_x emission and regional air quality remains
94 unclear.

95 In this study, we present a pulse of atmospheric NO_2 column in early spring during the past
96 two decades over the NCP. However, this phenomenon has not been previously reported in this
97 region. Combining agricultural fertilization records, surface NO_2 and NH_3 observations, long-
98 term satellite observations of NO_2 and NH_3, and a flexible scheme of soil NO_x emission, we
99 explain successfully the underlying cause for the NO_2 column peaks using a regional
100 atmospheric transport model online coupled with chemistry, and further assess the impacts of
101 the pulsing NO_x emission on reginal air quality.
102

103 ## 2 Materials and Methods

104 ### 2.1 Model and configurations

105 The Weather Research and Forecasting model fully coupled with atmospheric chemistry
106 (WRF-Chem, version 3.6.1) we used is a modified model by Li et al. (2011a; 2012; 2010;
107 2011b) and Feng et al (2021), in which we implement the BDSNP mechanism by Hudman et
108 al. (2012) to calculate soil NO_x emission related to agricultural fertilization and the influences
109 on regional air quality in the NCP. The model is configured with grid spacing of 6 km × 6 km
110 (240 × 280 grid cells) with the center at 38°N and 116°E (Figure 1). Thirty-five vertical levels
111 are employed in the stretched vertical grid with spacing ranging from 50 m near surface, to 500
112 m at 2.5 km and 1 km above 14 km. Meteorological initial and boundary conditions use the
113 National Centers for Environmental Prediction (NCEP) FNL 1°×1° analysis data, and the
114 chemical initial and boundary conditions are interpolated from the CAM-Chem 6-h output
115 (Buchholz et al., 2019; Emmons et al., 2020). The non-soil emission inventory is developed by
116 Zhang et al. (2009) and the biogenic emissions are calculated online using the Model of
117 Emissions of Gases and Aerosol from Nature (MEGAN) model (Guenther et al., 2006).

Specifically, monthly ammonia (NH_3) emissions are incorporated from a high-resolution NH_3 emission inventory developed by Huang et al., (2012), which includes emissions from fertilizer application, livestock, and other sources. The model spin-up time is 2 days (Table 1).

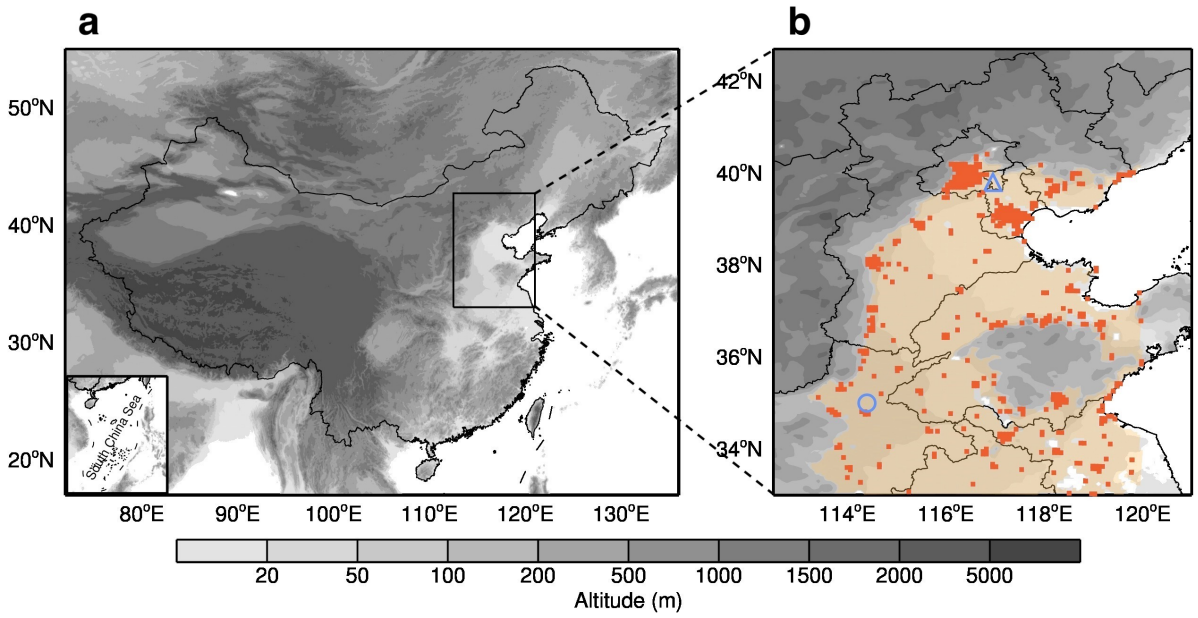

Figure 1. Domain overview. (a) Geographic location of the NCP, which is predominantly characterized by plains at an elevation less than 100 m, and known for a major agricultural zone. (b) Extensive cultivated croplands distribute in the NCP, marked by the orange shadings, while urban areas are marked by red shadings. The graphic markers denote locations of field observation sites, of which the blue circle represents the Fengqiu cropland ecological station, Chinese Academy of Sciences, with a long-term record on agricultural fertilization, and the triangle represents the rural Xianghe station with ambient NH_3 measurements. The agricultural areas in orange within the NCP are defined as croplands with altitude less than 100 m, and the urban areas in red are defined as built-up areas within the NCP.

Table 1. Model configuration for the simulation domain, meteorological schemes, initial and boundary conditions, and emission inventories.

Item	Configuration
Period	February through April, 2020
Region	The NCP and surrounding areas
Domain center	116°E, 38°N
Domain size	1440 km × 1680 km
Horizontal resolution	6 km × 6 km
Vertical resolution	35 vertical levels with a stretched vertical grid with spacing ranging from 50 m near surface, to 500 m at 2.5 km and 1 km above 14 km
Microphysics scheme	WRF Single-Moment 6-class scheme (Hong and Lim, 2006)
Boundary layer scheme	MYJ TKE scheme (Janjić, 2002)
Surface layer scheme	MYJ surface scheme (Janjić, 2002)
Land-surface scheme	Noah land surface model (Chen and Dudhia, 2001)
Longwave radiation scheme	New Goddard scheme (Chou et al., 2001)
Shortwave radiation scheme	New Goddard scheme (Chou and Suarez, 1999)
Meteorological boundary and initial condition	NCEP FNL 1° × 1° analysis data
Chemical boundary and initial condition	CAM-Chem 6-h output (Buchholz et al., 2019; Emmons et al., 2020)
Anthropogenic emission inventory	MEIC emission inventory (Li et al., 2017b; Zhang et al., 2009), except for NH_3
NH_3 emission inventory	NH_3 emission inventory in China (Huang et al., 2012)
Biogenic emission inventory	MEGAN model (2006)
NO_x emission from various types of soils	Soil NO_x emission mechanism (2012)
Spin-up time	2 days

2.2 Soil NO_X emission scheme

We implement a soil NO_x emission scheme, the Berkeley-Dalhousie Soil NO Parameterization (BDSNP) by Hudman et al. (2012), into the WRF-Chem model. The scheme comprehensively considers various factors, including available soil nitrogen content (N_{avail}, ng N m^{-2}) from the fertilizer application and nitrogen deposition, in which the soil NO_x emission (E_{soil}, ng N m^{-2} s^{-1}) is a function of N_{avail}, climate, and edaphic conditions:

$$E_{soil} = A'_{biome}(N_{avail}) \times f(T) \times g(\theta) \times P(l_{dry}) \quad (1)$$

where N_{avail} is available soil nitrogen mass, and A'_{biome} (ng N m^{-2} s^{-1}) represents the biome-dependent emission factor. $f(T)$ (dimensionless) and $g(\theta)$ (dimensionless) are parameters

regulated by soil temperature and moisture, respectively. $P(l_{dry})$ (dimensionless) denotes the pulsed soil emission from wetting of dry soils. The product by $f(T)$ and $g(\theta)$ is calculated following:

$$f(T) \times g(\theta) = e^{0.103T} \times a\theta e^{-b\theta^2} \quad (2)$$

where T ($0 \leq T \leq 30°C$) is soil temperature and θ ($0 \leq \theta \leq 1$, dimensionless) is water-filled pore space, defined as the ratio of the volumetric soil moisture content to the porosity. According to the laboratory and field measurements (Hudman et al., 2012), the constants a and b are determined so that $g(\theta)$ maximizes when $\theta = 0.2$ for arid soils and $\theta = 0.3$ elsewhere.

The pulsing term $P(l_{dry})$, following Yan et al. (2005), describes the magnitude of the peak flux relative to the pre-wetting flux, which is parameterized as:

$$P(l_{dry}) = [13.01 \ln(l_{dry}) - 53.6] \times e^{-ct} \quad (3)$$

where l_{dry} (hours) represents the length of the antecedent dry period, and c ($c = 0.068$ h^{-1}) is a constant rate denoting the rise/fall time of the pulse. Fertilizer applications data are interpolated from the global gridded chemical fertilizer and manure application inventory at 0.5°× 0.5° (Potter et al., 2010; Yan et al., 2005). The chemical and manure fertilizers are obtained from the International Fertilizer Association (IFA) and the Food and Agriculture Organization of the United Nations (FAO). The Chinese chemical fertilizer application (straight N application) from IFA is about 19.6 Tg N a^{-1} for 2000, quite close to the amount of 19.9 Tg N a^{-1} for 2020 from the China Statistical Yearbook (https://www.stats.gov.cn/sj/ndsj/2021/indexch.htm). More details of the scheme are found in related studies elsewhere (Hudman et al., 2012; Lu et al., 2021). It should be noted that we use the default BDSNP fertilizer and global emission assumptions, and these assumptions (primarily the 75/25 split and not applying the topdressing in a single application) may not accurately reflect the fertilizer applications in China. The BDSNP tuning, which was done for year 2000 agricultural emissions estimated by Stehfest and

Bouwman (2006), is close to recent estimates of global emissions, possibly on the high side (Gong et al., 2025; Wang et al., 2022b).

2.3 Emission inventories

We employ two emission inventories in this study, of which the Hemispheric Transport of Air Pollution Version 3 (HTAP v3, 2005-2018) emission inventory includes soil and non-soil emissions (Li et al., 2017a), and the Multi-resolution Emission Inventory for China (MEIC v1.3, 2007-2018) has no soil emission (Li et al., 2017a). In the HTAP inventory, the non-soil emission inventory includes energy, industry, ground transport, residential, waste, shipping and aviation sources in the HTAP inventory, with a spatial resolution of 0.1°×0.1° and a temporal resolution of one month. Agricultural emissions are involved in the latest HTAP v3 inventory, which includes soil NO_x emissions (Crippa et al., 2023). Nevertheless, the soil emissions in this inventory are calculated using traditional "bottom-up" method (Kurokawa and Ohara, 2020), rather than estimated by a process-based emission module. The monthly MEIC emission inventory with a spatial resolution of 0.25°×0.25° is incorporated in parallel with the HTAP emission inventory. Here, we focus on NO_x and NH_3 emissions from croplands with fertilization, and adopt NH_3 emission inventory by Huang et al. (2012) because they explicitly distinguish NH_3 produced by agricultural fertilization from other NH_3 sources.

2.4 Air pollutant measurements

Satellite-derived tropospheric NO_2 columns are from OMI hosted by the Aura satellite that is launched by the National Aeronautics and Space Administration (NASA). The Level-3 product, where pixel level data of good quality are binned and "averaged" into 0.25°×0.25° grids, was retrieved and analyzed in the present study. The satellite operates in a sun-synchronous polar orbit and has a local overpass time of around 13:45 (local time, LT) in North China. The dataset

is for all atmospheric conditions, and for sky conditions with cloud fraction less than 30% (https://cmr.earthdata.nasa.gov/search/concepts/C1266136111-GES_DISC.html). The dataset has a spatial resolution of 13 km × 24 km, with a temporal coverage of 2005-2022 (Lamsal et al., 2021). Note that the number of pixels included in NO_2 retrievals changes over time because of the increase in the number of pixels affected by the row anomaly issue, making the data unsuitable for trend analysis and possibly introducing uncertainty in seasonal averages. The Level-2 product of NH_3 columns is employed, which is from the Space Administration and the Infrared Atmospheric Sounding Interferometer (IASI) hosted on the MetOp series of satellites. The satellite also operates in a sun-synchronous polar orbit and has a local overpass time of around 9:30 am and 9:30 pm in North China (twice a day). We construct a 0.25° × 0.25° mesh grid and calculate the average of the NH_3 columns from IASI within each grid cell (Clarisse et al., 2023). Low-quality satellite data are filtered out due to the interference of clouds. To cover all the domain (Figure 1), the data used in this study are averaged into seven-day mean datasets of NO_2 and NH_3 columns with a non-overlapping 7-day window during 2007-2021. The data are interpolated into the model grids using bilinear interpolation.

Ambient surface NO_2, O_3, and $PM_{2.5}$ mass concentrations at 141 sites in the NCP are from the China National Environmental Monitoring Centre (CNEMC, Figure S1). These *in-situ* measurements are performed by the Thermo Scientific™ ambient particulate monitor and gas analyzers, of which NO_2 and O_3 are measured by Model 42i Chemiluminescence NO-NO_2-NO_x Analyzer, Model 49i UV Photometric Ozone Analyzer, respectively. $PM_{2.5}$ is measured by Model 5030 Synchronized Hybrid Ambient, Real-time Particulate (SHARP) Monitor, which uses proprietary digital filtering to continuously calibrate mass to obtain an accurate, precise and real-time mass concentration. The sampling time is 1 min for these monitoring devices. Agricultural NH_3 concentration is monitored by a Picarro analyzer based on the principle of

cavity ring-down spectroscopy (CRDS) at the rural Xianghe station (Figure 1), with a sampling frequency of 1 Hz. Hourly data are derived by averaging the high-frequency measurements.

3 Results and Discussion

3.1 Satellite-retrieved NO_2 column pulses

During the past two decades, seven-day mean tropospheric column of NO_2 measured by the Ozone Monitoring Instrument (OMI) in the NCP exhibits a significant temporal variation, with the magnitude varying from less than 100 μmol m^{-2} to more than 680 μmol m^{-2} (Figure 2a). The annual cycle is highly prominent and its seasonal variation is remarkable, with significantly higher levels in cold seasons than those in warm seasons. Throughout the year, the pattern of NO_2 column looks like a rhinoceros horn, which is characterized by a major peak in winter and multiple noticeable sub-peaks in other seasons. These sub-peaks often occur at fixed times, such as in March, June and October, of which the sub-peak is the most noticeable in March, with the highest magnitude (Figures 2a and S1). We examine the monthly variation in anthropogenic NO_x emission rates over the NCP in global and regional emission inventories, and find that the monthly variation is more evident in the regional emission inventory, with a significantly higher emission than that in the global emission inventory. Nevertheless, neither of them reveals any discernible sub-peaks of NO_x emission rates from fossil fuel combustion to coincide with the sub-peaks of the NO_2 column (Figure 2b).

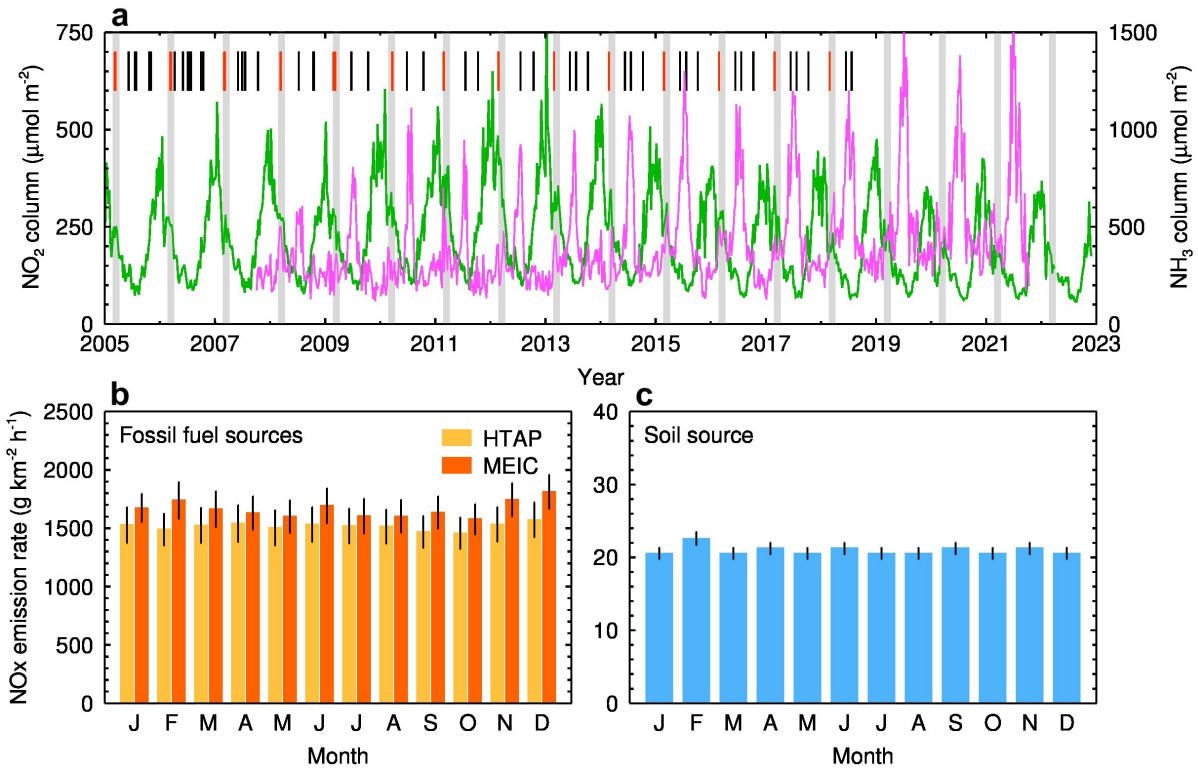

Figure 2. NO_2 column pulses in March, NH_3 column variation, and NO_x emissions from fossil fuel and soil sources over the NCP. (a) Long-term variation of seven-day mean tropospheric NO_2 column observed by OMI during 2005-2022 (green) and NH_3 column retrieved from IASI during 2007-2022 (pink). Intersections of the gray bars and the green lines denote a sub-peak of NO_2 column occurred in each March, and the short bars represent the timing record for agricultural fertilization at Fengqiu station in the NCP, of which the red ones indicate the fertilization period in early spring. (b) Monthly mean NO_x emission rates with $\pm 1\boldsymbol{\sigma}$ standard deviation (SD) in two sets of anthropogenic emission inventories, the HTAP v3 (2005-2018, orange) and MEIC v1.3 (2008-2017, red). (c) Same as (b), but for NO_X emission rates from soils in the HTAP v3 inventory (2005-2018).

As for soil NO_x emissions, they are absent in the regional emission inventory, while in the global emission inventory, soil NO_x emissions fluctuate slightly on a monthly scale, far less than those from fossil fuel combustion, constituting less than 2% of the total (Figure 2c).

Similar to NO_x emissions from fossil fuel combustion, there are no evident sub-peaks of soil NO_x emission to keep pace with the atmospheric NO_2 column. Soil NO_x emissions are even at a lower level in March, significantly less than emissions in adjacent months. Therefore, the known emission inventory fails to explain the occurrence of these sub-peaks. On the other hand, we compute a pollution accumulation index (PAI, Text S1), the product of boundary layer height and wind speed, to semi-quantitatively assess the influence of atmospheric dispersion conditions on NO_2 column. NO_2 column seems to be somewhat dependent on the PAI, yet the noticeable discrepancies between the timing of the sub-peaks and PAI are insufficient to account for the occurrence of each sub-peak (Figure S3). Additionally, it is seen that the daily soil temperature was consistently higher than 0°C during March 2020 and the ten days before (Figure S4). Therefore, the sub-peak of NO_2 column is not expected to be originated from soil thaw either.

3.2 Linkage between NO_2 column pulses and agricultural fertilization

What causes these regular NO_2 sub-peaks occurred over the NCP during the past two decades? Measurements on ammonia (NH_3) column also present similar pulses to those of NO_2 column during the same period, in spite of some differences in the long-term trend (Figure 2a). Although the main peaks of NH_3 column occur in June, the sub-peaks of NH_3 column in March may provide favorable evidence that these NO_2 column sub-peaks are connected to agricultural activities because atmospheric NH_3 is largely originated from fertilizer application in agriculture (Crippa et al., 2023; Huang et al., 2012; Li et al., 2017a). We note that the two time series don't have similar seasonal dynamics, which may raise some questions about whether the March NO_2 peaks represent fertilizer pulses. This discrepancy could be due to several factors: (1) contributions from fossil fuel-derived NO_x, (2) elevated background soil NO_x emissions during the "spring thaw" period, (3) differences in fertilizer type, as fertilizers vary

277 in their potential for ammonia volatilization, and (4) variation in application methods, e.g.,
278 banding or deep soil placement *vs* broadcasting, especially when the latter is done without
279 incorporation.

280 Another key evidence is that the occurrence of each sub-peak of the NO_2 column is highly
281 consistent with the record of agricultural fertilization at the Fengqiu cropland ecological station
282 in the NCP during the past decades (Figures 1b, 2a, and S1). The wheat-maize double-cropping
283 system is predominate in the NCP, where the agricultural activities are strongly dependent on
284 the lunar calendar. For winter wheat, the planting date ranges from early to mid-October (after
285 maize harvest). Fertilization is generally divided into three stages: 1) Pre-planting during late
286 September – early October; 2) Jointing stage during mid-March – early April; 3) Grain filling
287 during late April for high-yield fields. The planting date of summer maize ranges from early to
288 mid-June (after wheat harvest), and the stages of fertilization include: 1) At planting during
289 early June; 2) V6-V8 stage during early July; 3) Tasseling stage during late July for high-yield
290 fields. The agricultural fertilization is closely associated with three solar terms, i.e., Waking of
291 Insects in March (the 3rd solar term), Grain in Beard in June (the 9th solar term) and Cold Dew
292 in October (the 17th solar term). During these pulses of the NO_2 column, we found that the
293 pulse in March is more pronounced than those in June and October, because March is the
294 season for a large-scale cultivating in the NCP, accompanied by more land preparation and
295 fertilization. Therefore, we hypothesize that the NO_2 column pulse in March is possibly caused
296 by fertilized croplands that accelerate NO_x emissions from agricultural soils. Field campaigns
297 have measured a high NO emission rate of 266.3 g km^{-2} h^{-1} in croplands after fertilization and
298 irrigation in autumn in eastern China (Tang et al., 2020; Tian et al., 2020) and also other regions
299 (Hickman et al., 2017; Huang et al., 2018; Huber et al., 2020), suggesting that agricultural
300 fertilization is likely a significant source of atmospheric NO_x in major agricultural countries
301 like China.

3.3 Soil NO_x emission mechanism

To examine the role of soil NO_x emissions from agricultural fertilization in the pulses of atmospheric NO_2 column, we introduce a flexible soil NO_x emission module and NH_3 emission into the WRF-Chem model, and perform two simulation experiments that include and exclude soil emissions, respectively (Table 1). Noticeably, there is an acceleration in the release of soil NO_x, and daily mean emission rate increases from 155.6 g km^{-2} h^{-1} to 438.3 g km^{-2} h^{-1} during the simulation period (Figure 3a). In particular, the NO_x emission rate during the post-fertilization phase is significantly higher than those during other phases, consistent with the accelerated soil NO_x release observed in agricultural areas in California after fertilization (Oikawa et al., 2015). On average, the simulated NO_x emission rate in March is 312.9 g km^{-2} h^{-1}, between the measured 113.6 g km^{-2} h^{-1} in November in eastern China (Tang et al., 2020) and 988.2 g km^{-2} h^{-1} in September in California (Oikawa et al., 2015), suggesting the rationality of the soil NO_x emission mechanism in the model. We should also note that the BDSNP scheme would be heavily biased towards having a fertilizer-induced emission peak only at planting/green-up.

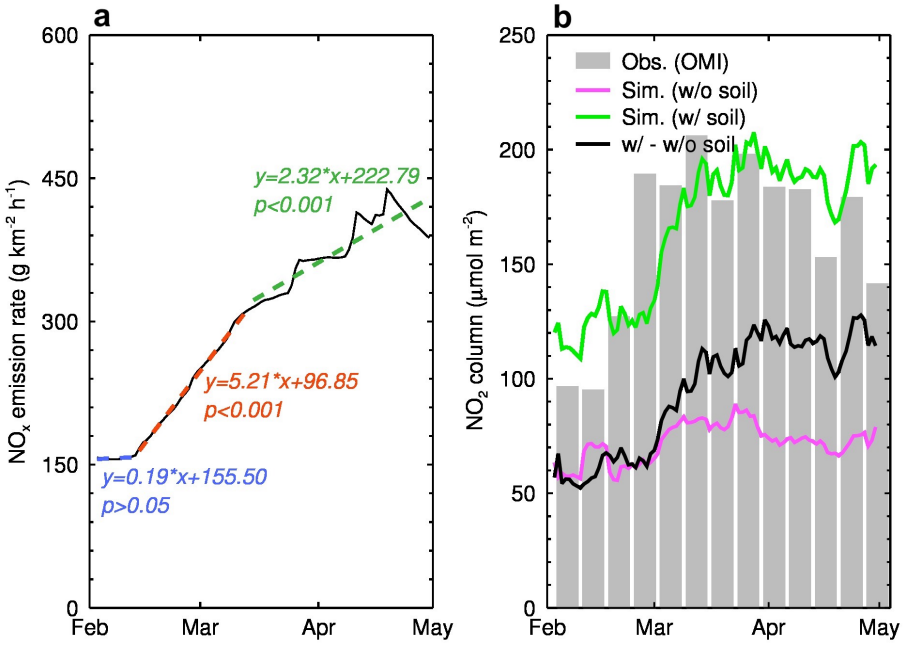

Figure 3. NO_x emissions from agricultural fertilization and resultant NO_2 column during February-April in 2020 over the NCP. (a) Calculated NO_x emission rate from croplands with N-fertilizer application in the model. The black curve represents daily variation in NO_x emission rate around the fertilization, and the blue, red, and green dash lines correspond to the trends of NO_x emission rates in croplands during the pre-fertilization, fertilization and post-fertilization periods, respectively. (b) Observed and simulated NO_2 column. The gray histogram represents NO_2 column observed by satellite (OMI). The green and pink lines represent simulated NO_2 column with and without soil NO_x emissions, and the black line shows the difference between them. The model well replicates the rapid increase in observed NO_2 column by considering soil NO_x emissions from agricultural fertilization.

We evaluate the model performance against satellite-derived NO_2 column. Consequently, the modified model perfectly replicates the sudden increase in NO_2 column linked to agricultural fertilization, while the conventional WRF-Chem model fails to capture the observed NO_2 column pulse in March due to lack of the adopted soil NO_x emission mechanism (Figure 3b). For example, when soil NO_x emission caused by agricultural fertilization is considered, the simulated NO_2 column rapidly increases to the peak in March, matching well with the satellite observation. However, without the contribution of agricultural fertilization, NO_2 column seems to exhibit a weak upward trend, but not significant. Comparing these two scenarios, a substantial NO_x emission from N-fertilizer input in croplands leads to an increase in NO_2 column by 1 to 1.5 times.

We also validate the modified model performance on temporal variations of routine surface pollutant measurements (NO_2, O_3 and $PM_{2.5}$) associated with NO_x emissions at the CNEMC sites throughout the simulation period (Figure 4). Although there are some discrepancies between the simulations and observations, e.g., overestimates occur in mid-

February for NO_2 and $PM_{2.5}$ levels, the model generally reproduces hourly variations in each pollutant reasonably. The indices of agreement (IOAs, Text S2) between the simulated and observed near-surface concentrations of NO_2, O_3, and $PM_{2.5}$ are 0.90, 0.91, and 0.88, respectively, and the normalized mean biases (NMBs) for these pollutants are within 10%.

We still cannot ignore the discrepancies between the model results and observations. These biases may largely originate from the soil NO_x emission mechanism. The fertilization dates in the BDSNP mechanism are determined by the beginning and end of the growing season that is derived from the MODIS Land Cover Dynamics product (MCD12Q2) averaged over the years from 2001 to 2004 (Hudman et al., 2012). This may be quite different from practices in 2020, the year we simulated in this study. We use the default assumption in the mechanism that 75% of fertilizer is added at the green-up day with the remaining 25% applied constantly throughout the rest of the season (Hudman et al., 2012). We should note that the 75/25 treatment is an estimate for local farming practice in Mexico in 1994 (Matson et al., 1998), which probably introduces biases in other regions. Typical practice would place more fertilizer at topdressing and less at planting. For example, a 20/80 split was used by GGCMI, the largest global crop modeling exercise (Jägermeyr et al., 2021), and a 40/60 split was used for maize production in Northeast China (Zheng et al., 2023). It's also worth noting that the BDSNP mechanism treats topdressing as a series of applications spread out over several weeks or months, rather than as a single event, which could further influence the modeling results. Despite the uncertainties, all of these significant improvements of the modified model we used suggest that soil NO_x emission from agricultural fertilization would exert a crucial influence on regional air quality.

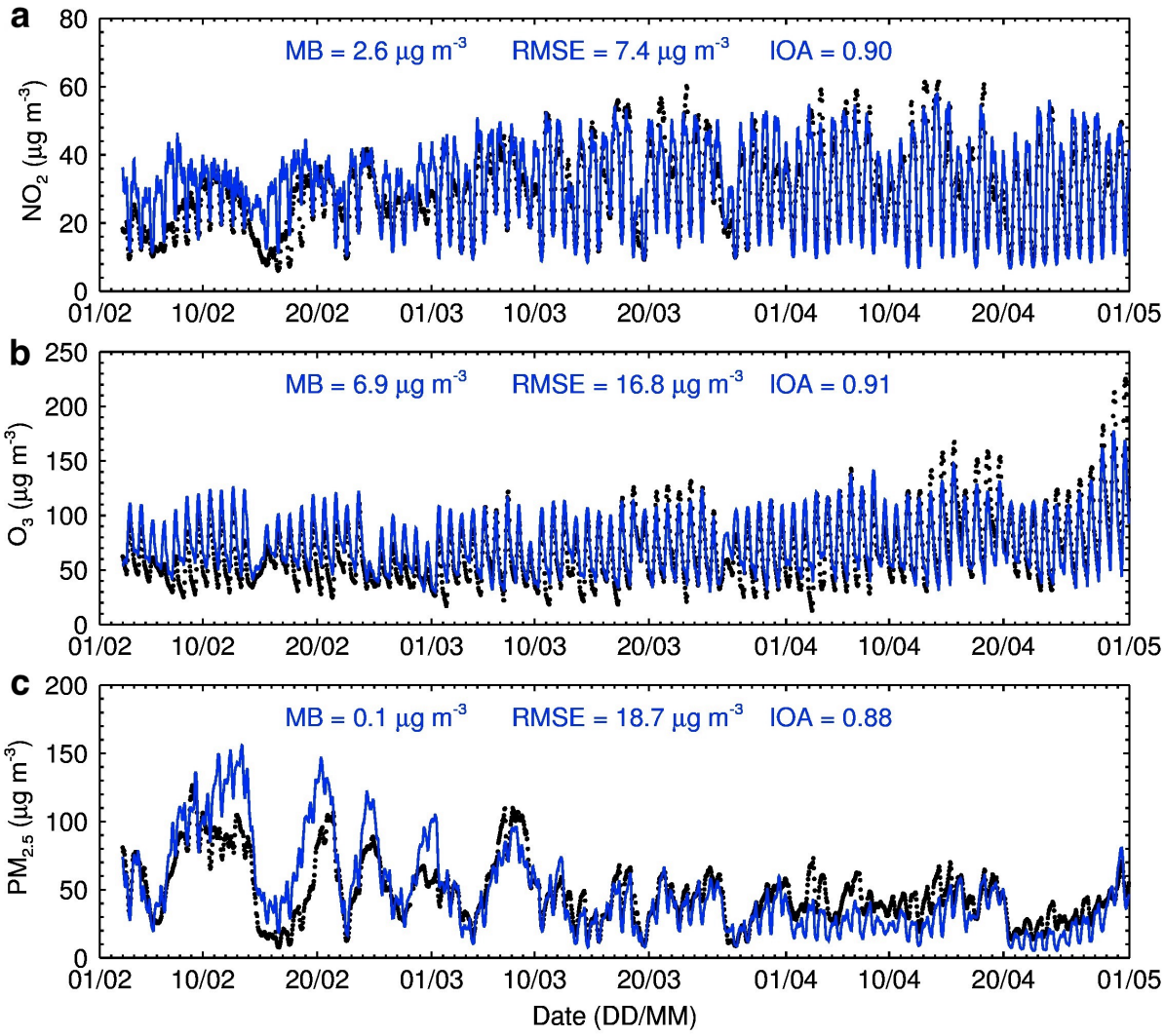

Figure 4. Simulated *vs.* measured surface pollutants averaged over the monitoring sites of the NCP (Figure S1) during February-April in 2020. (a to c) Temporal variations in surface NO_2 (a), O_3 (b), and $PM_{2.5}$ (c) mass concentrations. The blue curves denote the model calculation and the black dots denote *in-situ* measurements. Model biases are shown in the central upper position of each figure.

Furthermore, we examine the ability of the model to simulate the ground-level NO_2 mass concentration and NH_3 volume concentration when soil NO_x rapidly releases after fertilization. The reason is that influences of soil emissions on atmospheric NO_2 and NH_3 concentrations are confined in the near-surface layers below 1 km, and the influences diminish rapidly as

377 altitude increases (Figure 5). This indicates that impact of the soil emissions is primarily
378 concentrated near the ground surface. With soil emissions included or not in the model, we
379 compare the simulated NO_2 and NH_3 concentrations with near-surface observations (Figures
380 6a and 6b). When there are no soil NO_x emissions from agricultural fertilization, the simulated
381 NO_2 concentration is significantly lower than the observed by 9.4 μg m^{-3} during February
382 through April, 2020. While considering these emissions, the mean bias (MB, Text S2) between
383 the simulation and the observation decreases to 2.6 μg m^{-3}, and the IOA also increases from
384 0.48 to 0.78. Similarly, the simulated NH_3 concentration is in good agreement with the
385 observed when the soil NH_3 emission related to agricultural fertilization is involved, e.g., the
386 MB decreases from -12.0 ppb to -4.4 ppb, and the IOA increases from 0.56 to 0.64 (Figures 6c
387 and 6d). It is important to acknowledge the limitation posed by the absence of direct
388 comparisons with flux measurements of NO_x emissions from soils, due to the unavailability of
389 such data. The simulated NO_x emission flux from the BDSNP scheme cannot be well examined,
390 which may introduce uncertainties to the predicted emission rates and mixing ratios in the
391 atmosphere.

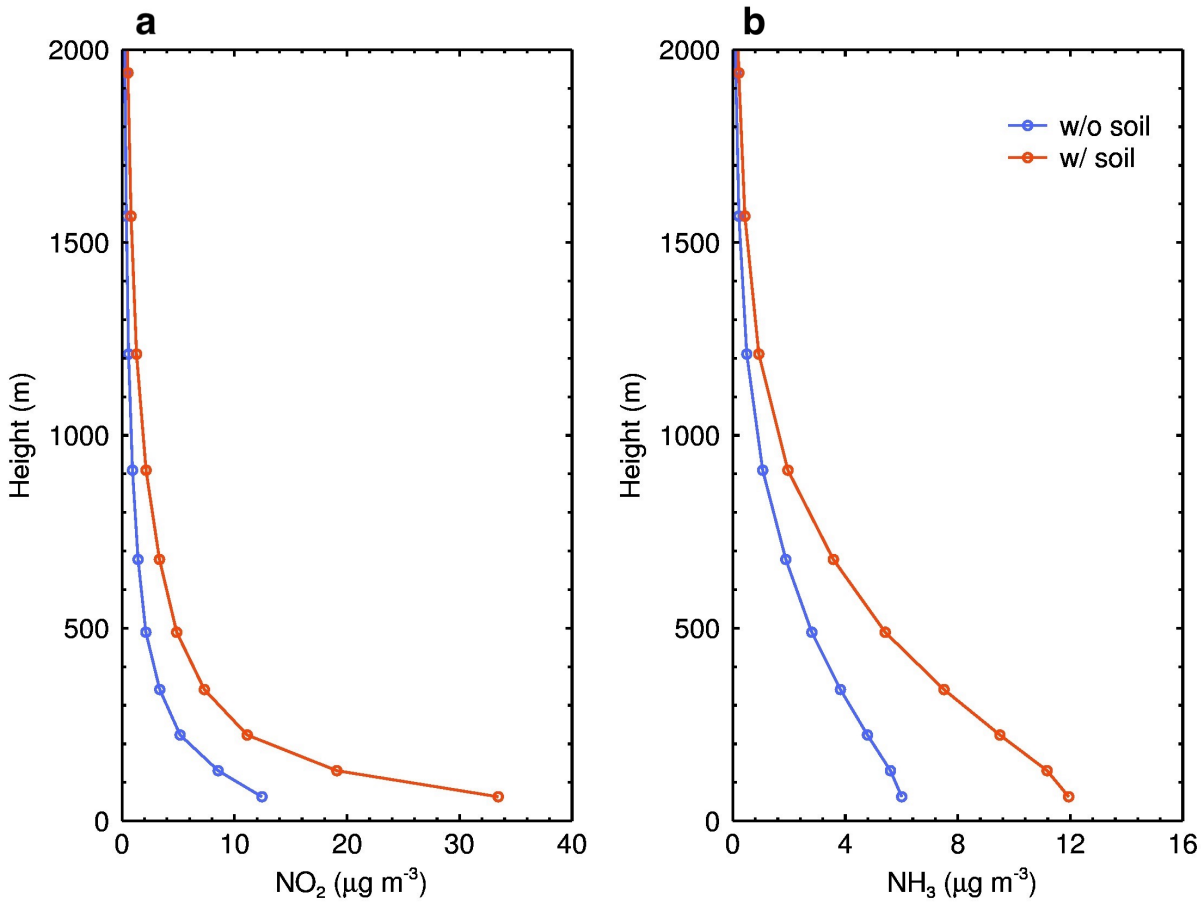

392

393 Figure 5. Vertical profiles for impacts of soil emissions on gas pollutants during March 2020

394 over the NCP. (a) Difference in NO_2 concentration with and without the influence of soil NO_x

395 emission from agricultural fertilization at various heights in the near-surface layers. (b) Similar

396 to (a), but for NH_3 concentration.

397

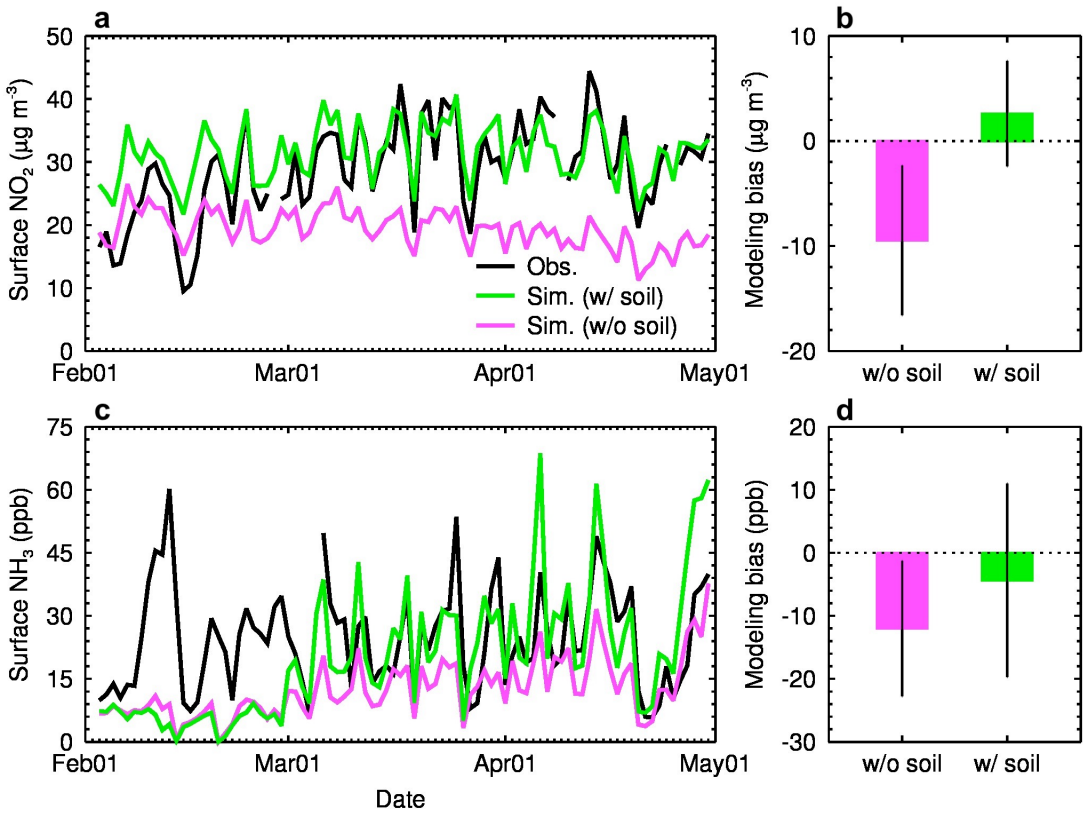

Figure 6. Contribution of soil emissions from agricultural fertilization on surface NO_2 and NH_3 during February through April 2020 over the NCP. (a-b) Change in surface NO_2 concentration with (green) and without (pink) soil NO_x emission from agricultural fertilization, the black line in (a) is for observed surface NO_2 concentration. (c-d) Same as (a-b), but for NH_3. The error bar in (b and d) denotes $\pm 1\boldsymbol{\sigma}$. NO_2 observations are averaged over the 141 monitoring stations in the study area from the CNEMC network. NH_3 observations are from the rural Xianghe station (Figure 1). According to *in-situ* measurements on NO_2 and NH_3, the units for NO_2 and NH_3 concentrations are μg m^{-3} and ppb, respectively.

3.4 Significance of soil NO_x emissions from agricultural fertilization for air quality

We perform a model experiment that excludes the soil sources of NO_x and NH_3 in the study domain to examine the impacts of soil emissions on regional air quality. The model results are compared to the benchmark scenario with soil sources involved to examine these impacts. Agricultural fertilization directly leads to substantial increases in atmospheric NO_x and NH_3

concentrations. According to the spatial correlation between land use and NO_2 concentration, NO_2 concentrations increase by more than 15 μg m^{-3} over agricultural areas, with the maximal increments occurring in the densely cultivated southern region of the NCP, exceeding 40 μg m^{-3} (Figures 1b and 7a). While in urban areas, the increase in NO_2 concentration is mostly below 10 μg m^{-3}, significantly lower than those in agricultural areas. This indicates that the influence of local emissions originated from agricultural fertilization on air quality primarily concentrate in agricultural areas. Nonetheless, the influence extends to surrounding areas through atmospheric transport, leading to an inhomogeneous increase of NO_2 concentrations across the NCP. Spatial distribution of the increased NH_3 concentration is highly similar to that of the increased NO_2 concentration, but some differences exist in the southeast of the NCP. It should be noted that the NH_3 emission in the model is from Huang et al. (2012), a separate monthly emission inventory. The emission rates of NH_3 in the southeast of the NCP is lower than that of NO from the BDSNP scheme. This indicates nonnegligible discrepancies in the derived emissions between these two approaches, which deserves more in-depth studies.

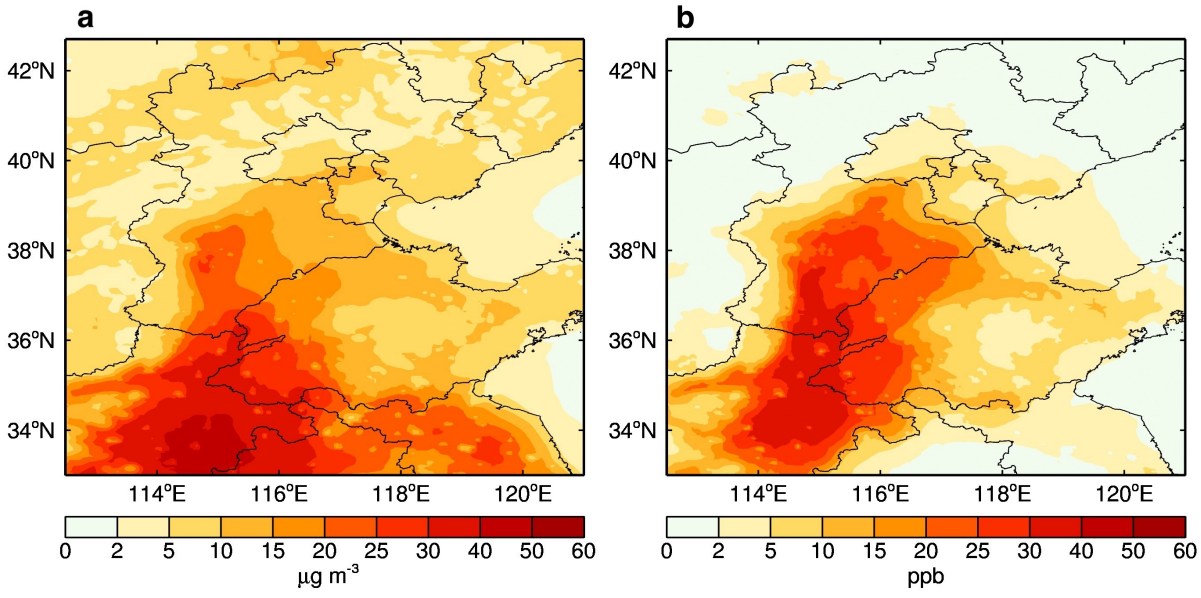

Figure 7. Direct impacts of soil emissions from agricultural fertilization on (a) surface NO_2 and (b) NH_3 during March 2020 over the NCP. (a and b) Spatial distributions of changes in surface NO_2 and NH_3 concentrations due to fertilization-related soil emissions. According to *in-situ*

measurements on NO_2 and NH_3, the units for NO_2 and NH_3 concentrations are μg m^{-3} and ppb, respectively.

A substantial amount of reactive nitrogen from agricultural fertilization suddenly enters the atmosphere, and further affects air quality via photochemical reactions and aerosol chemical transformations profoundly (Seinfeld and Pandis, 2006; Wu et al., 2020). Our results reveal that the NO_x emission induced by N-fertilization significantly suppresses the early-spring O_3 production in the NCP, which varies remarkably with the land use, approximately twice as strong in agricultural areas as in urban areas. For instance, in agricultural areas, the emission in croplands reduces nocturnal and diurnal O_3 by 30.1±6.5 μg m^{-3} (37.5±8.1%) and 15.0±3.7 μg m^{-3} (18.7±4.6%), respectively, while in urban areas, the corresponding O_3 reductions are 15.6±4.7 μg m^{-3} (15.6±4.7%) and 9.7 ±3.2 μg m^{-3} (10.6±3.4%), respectively (Figure 8). Based on the diurnal cycle of the change in O_3 concentrations ($\Delta[O_3]$), we also find that the nighttime O_3 reduction is much higher than the daytime reduction (Figure 9). The $\Delta[O_3]$ caused by agricultural fertilization is linearly and negatively correlated with the change in NO_2 concentration ($\Delta[NO_2]$) (Figures 10a-d), and the negative correlation is more pronounced at night ($r < -0.99$ and $p < 0.001$ for both the agricultural and the urban areas, Figures 10a and b). This suggests that the O_3 concentration strongly depends on the change in NO_x levels in the NCP during early spring. Continuous agricultural NO_x (mainly NO) emissions inhibit the O_3 formation, which indicates that the NO_x abundance is excess for O_3 formation over the NCP. Huang et al., (2023) similarly reported that variations in O_3 concentrations were inversely related to the changes in soil NO_x emissions in the NCP. Lu et al., (2021) also reported a NO_x-saturated O_3 formation regime in the NCP. On the other hand, a negative correlation between $\Delta[NO_2]$ and the change in daytime OH radical ($\Delta[OH]_{day}$) suggests that the $\Delta[NO_2]$ also moderately regulates $\Delta[OH]_{day}$ ($r = -0.50$ for agricultural areas and $r = -0.43$ for urban areas, p

< 0.001, Figures 10e and f) through decreasing O_3 levels and reactions of NO_2 with OH radical. Both OH radical and O_3 are critical oxidants in the atmosphere, and the decrease by the excessive NO_x emission from agricultural fertilization weakens atmospheric oxidizing capacity (AOC) (Feng et al., 2021). The decreased AOC can further slow down the oxidation processes in homogeneous and heterogeneous reactions, unfavorable for the formation of secondary aerosols. We note that soil nitrous acid (HONO) emission, which are not included in these modeling experiments, can also perturb atmospheric chemistry and the AOC (Feng et al., 2022; Tan et al., 2023) via providing NO and OH through photolysis. The emission rate of HONO from soil is much less than that of NO_x in the NCP (Tan et al., 2023), which increases daytime O_3 and OH concentrations slightly during summer (Feng et al., 2022; Tan et al., 2023). However, the influence in springtime still remains to be elucidated.

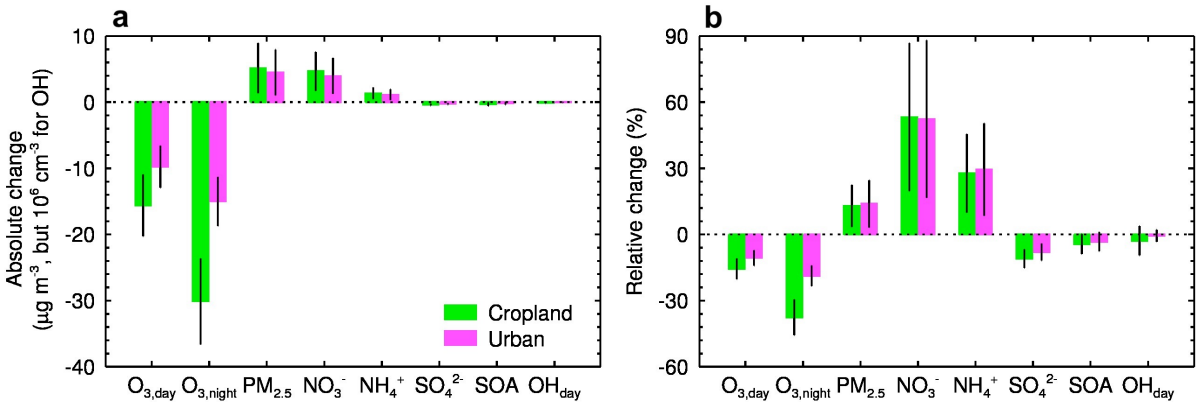

Figure 8. Complex impacts of agricultural fertilization on O_3, $PM_{2.5}$, and OH during March 2020 over the NCP. (a) Changes in mass concentrations of O_3, $PM_{2.5}$, aerosol constituents, i.e., nitrate, ammonium, sulfate and secondary organics, and OH radical due to soil NO_x emission from agricultural fertilization in agricultural (green) and urban (pink) areas. The error bar denotes $\pm 1\boldsymbol{\sigma}$. (b) Same as (a), but for percentage changes.

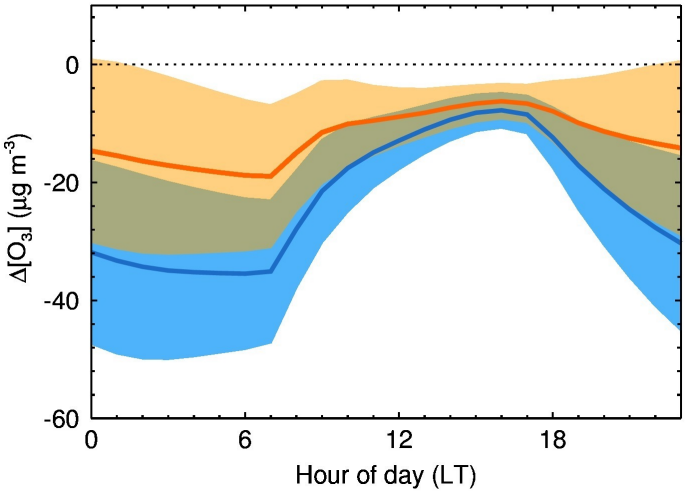

Figure 9. Secondary impact of soil NO_x emissions from agricultural fertilization on surface O_3 during March 2020 over the NCP. Diurnal cycles of changes in surface O_3 concentrations due to fertilization-related soil emissions over croplands and urban areas in the NCP. The blue and orange shadings show ±1**σ** of the data.

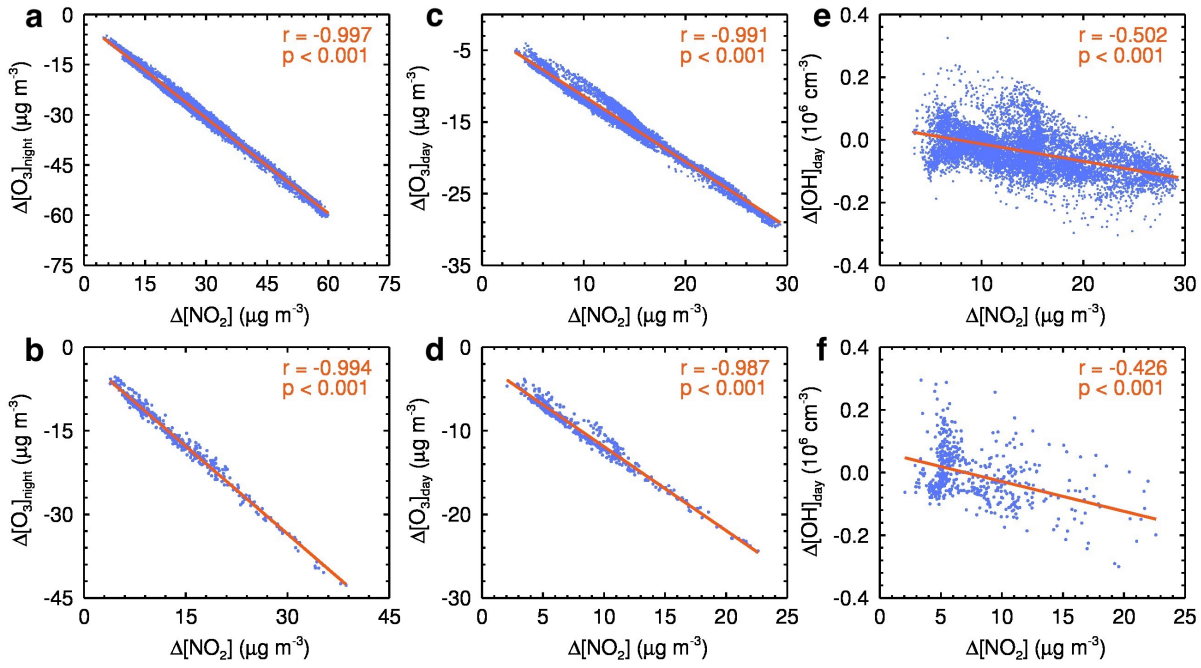

Figure 10. Changes in surface NO_2 and related photochemical products. (a to f) Correlation between $\Delta[NO_2]$ and $\Delta[O_3]$ or $\Delta[OH]$ during March 2020 over the NCP. (a to d) Change in O_3 concentration is strongly dependent on change in NO_2 concentration due to agricultural fertilization in both agricultural (a and c) and urban (b and d) areas, and the dependence is more

pronounced at night, i.e., correlation coefficient r = -0.997 (r = -0.994) at night and r = -0.991 (r = -0.987) at daytime in agricultural (urban) areas. (e and f) Change in daytime OH radical is also significantly influenced by change in NO_2 concentration in both agricultural (e) and urban (f) areas.

Interestingly, these findings regarding the impacts of soil NO_x emission on O_3 formation in spring are different from previous studies revealing that agricultural NO_x emissions enhance the O_3 formation in summer over the NCP (Tan et al., 2023; Wang et al., 2022a) and northeast China (Shen et al., 2023) and in the Imperial Valley, California (Oikawa et al., 2015). Similar scenarios are also reported during the growing season of crops in sub-Saharan Africa (Hickman et al., 2017; Huang et al., 2018). This is largely attributed to the sensitivity of O_3 to its precursors. During early spring, a large amount of agricultural NO_x (mainly NO) emission causes a NO titration effect during daytime, decreasing O_3 concentrations, when the O_3 chemistry is under the VOC-sensitive (NO_x-saturated) or the transitional regimes (Figure S6) (Sillman, 1995). In contrast, the O_3 formation chemistry in summer shifts from VOCs-sensitive to NO_x-sensitive (Sha et al., 2021; Wang et al., 2022a). In this scenario, the O_3 production is primarily controlled by NO_x emissions, meaning that the O_3 concentration increases with rising NO_x levels. This seasonal difference in O_3 sensitivity to its precursors highlights a seasonally dependent response of O_3 production to agricultural fertilization.

We also quantify the impact of agricultural fertilization on $PM_{2.5}$ concentrations. The NCP is characterized by an excess of NH_3, in which nitrate formation is highly sensitive to NO_2 concentration and AOC due to NO_2 oxidation to NO_3^- via gas-phase and heterogeneous reactions (Feng et al., 2018; Fu et al., 2020; Liu et al., 2019; Wen et al., 2018). As atmospheric NO_2 and NH_3 concentrations rapidly increase due to emissions from fertilized croplands, nitrate aerosol in agricultural (urban) areas rises by 4.7 (4.0) μg m^{-3}, corresponding to the

increased percentage of 53.2% (52.3%), while ammonium aerosol rises by 1.3 (1.1) μg m^{-3} in agricultural (urban) areas, with an increased percentage of 27.7% (29.4%) (Figure 8). However, sulfate aerosol shows a slight decrease both in agricultural and urban areas (Figure 8a). The reason is that an extra NO_x emission from agricultural fertilization enhances nitrate formation but lowers AOC, which hinders sulfate formation. Similar to sulfate aerosol, secondary organic aerosol (SOA) also has a slight reduction (Figure 8a). The formation of SOA greatly depends on the AOC level, so decreased AOC due to NO_x emission from agricultural fertilization does not favor the conversion of organic precursors, such as VOCs and semi-volatile primary organic aerosols, into SOA.

In general, due to the NO_x emission from agricultural fertilization, $PM_{2.5}$ concentration increases by 5.1 (4.5) μg m^{-3} (Figure 8a), corresponding to a percentage change of 12.9% (13.9%) over agricultural (urban) areas in the NCP (Figure 8b). There is no significant difference in $PM_{2.5}$ increments between agricultural and urban areas. Nitrate aerosol is primarily responsible for the increased $PM_{2.5}$, accounting for 92.2% and 88.9% in these two types of regions, respectively. Our results also indicate that changes in $PM_{2.5}$ and nitrate in urban areas are more sensitive to the change in NO_2 concentration. For instance, the ratios of nitrate change to NO_2 change ($\Delta[NO_3^-]/\Delta[NO_2] = 0.20$) and $PM_{2.5}$ change to NO_2 change ($\Delta[PM_{2.5}]/\Delta[NO_2] = 0.24$) in urban areas are both higher than those in agricultural areas ($\Delta[NO_3^-]/\Delta[NO_2] = 0.13$ and $\Delta[PM_{2.5}]/\Delta[NO_2] = 0.15$, Figures 11a and b), indicating that the conversion of NO_2 to nitrate aerosol is more efficient in urban areas. Consequently, the increased percentages of $PM_{2.5}$ and ammonium aerosol in urban areas are higher than those in agricultural areas (Figure 8b). Additionally, the ongoing stringent control measures on emission sources significantly reduce anthropogenic emissions in urban areas, thus the impact of agricultural fertilization on urban air quality is becoming more pronounced (Figure S7). Since soil NO_x emission is sensitive to soil temperature, as global warming is ongoing, routine events

like agricultural fertilization will continue to have amplified impacts on air quality with the joint help of atmospheric dispersion/transport and chemical transformation processes (Bennetzen et al., 2016; Ma et al., 2022; Tubiello et al., 2013). These impacts are not confined in agricultural areas alone, but extend to surrounding cities.

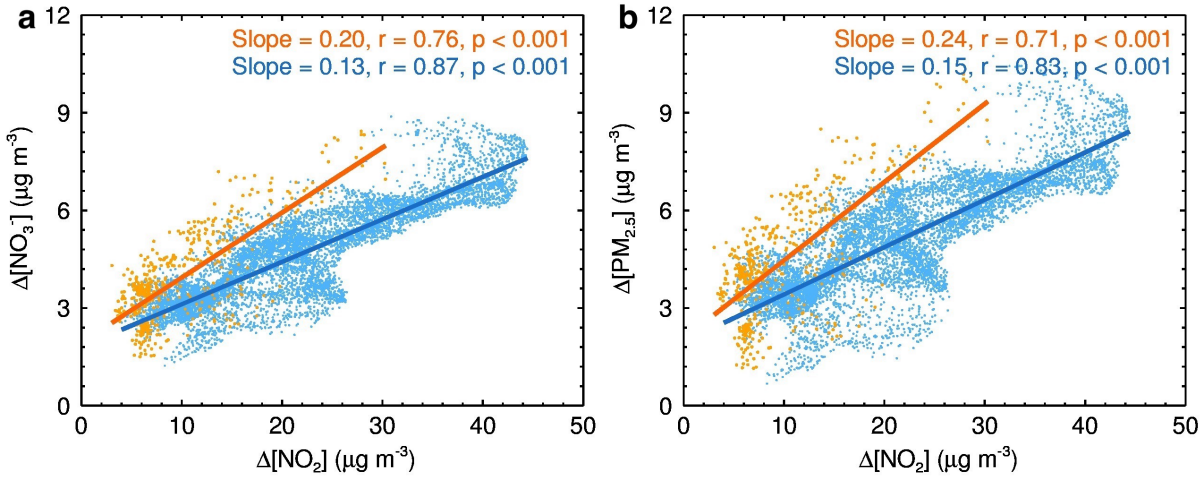

Figure 11. Simulated changes in surface NO_2 and related aerosol-chemistry products during March 2020 over the NCP. (a) Comparison of NO_2 conversion to nitrate aerosol (NO_3^-) formation between agricultural and urban areas, i.e., $\Delta[NO_3^-]/\Delta[NO_2] = 0.20$ in urban areas and $\Delta[NO_3^-]/\Delta[NO_2] = 0.13$ in agricultural areas, indicates that change in nitrate in urban areas are more sensitive to the change in NO_2 concentration and NO_2 conversion to NO_3^- is more efficient. (b) NO_2 conversion to $PM_{2.5}$ formation is similar to (a), because nitrate aerosol is the most affected among the various aerosol constituents. The blue and orange colors correspond to the agricultural and urban areas, respectively.

4 Conclusions and Implications

Impact of soil NO_x emissions from agricultural fertilization on the atmospheric environment remains unclear worldwide (Guo et al., 2020; Huang et al., 2018; Sha et al., 2021; Shen et al., 2023). In particular, this issue has not yet received enough attention in China, where substantial N-fertilizers are year by year consumed due to extensive agricultural cultivation areas (Sun et

552 al., 2022; Vitousek et al., 2009; Zhao et al., 2006). Our results indicate that agricultural
553 fertilization is highly responsible for the periodic pulse of the atmospheric NO_2 column in the
554 NCP over the past two decades. A two-decade record of fertilization events at a research station
555 and model results both provide evidence consistent with a cause-to-effect relationship. For
556 example, the fertilization timing is found to match well with the occurrence of satellite-derived
557 NO_2 column pulse in the region. Moreover, the model reasonably captures the regular sub-peak
558 of the NO_2 column in March by introducing an independent module that specifically describes
559 soil NO_x emissions from agricultural fertilization.

560 These additional NO_x emissions released by croplands directly lead to an elevated level of
561 surface NO_x concentrations. Consequently, the increased atmospheric NO_x concentration
562 significantly inhibits O_3 production in early spring, distinct from the impacts in summer (Sha
563 et al., 2021; Wang et al., 2022a), but enhances nitrate formation. For example, soil emissions
564 linked to agricultural fertilization dramatically reduce nighttime O_3 concentrations by 30.1 μg
565 m^{-3} and 15.0 μg m^{-3} in croplands and urban areas, respectively. During daytime, the decreased
566 O_3 concentration is 15.6 μg m^{-3} and 9.7 μg m^{-3}, respectively. In contrast, soil emissions elevate
567 ambient $PM_{2.5}$ concentrations by more than 4.5 μg m^{-3}, accounting for 12% of the $PM_{2.5}$ mass
568 over the NCP in March 2020. The opposite effects are challengeable for China to improve air
569 quality, because China is the world's largest consumer of food, of which food production
570 strongly depends on N-fertilizers input. As the emission from fossil fuel combustion has been
571 gradually decreasing, emissions from agricultural fertilization are with increasing implications
572 for air quality. We thus highlight that reducing NO_x emissions from agricultural fertilization is
573 of great importance to air quality improvement. In China, the excessive use of N-fertilizer still
574 remains severe (Sun et al., 2022; Vitousek et al., 2009; Zhao et al., 2006), though a lot of efforts
575 have taken to increase the N-fertilizer efficiency and to reduce N losses from fertilizer (Li et
576 al., 2018; Qiao et al., 2022; YAN et al., 2008). Fortunately, the consumption of N-fertilizer

reached its peak in 2014 in China and has been decreasing since then (Yu et al., 2022). Policymakers should manage to further reduce emissions from N-fertilizers application, for example, improving N-fertilizers efficiency and developing alternative fertilizers friendly to the environment are highly necessary. These measures will greatly minimize the adverse effects of agricultural fertilization on air quality, human health, and the ecological environment. Nevertheless, one should be aware of the limitation in the present case study that there are only three months of simulation as the basis for all of the insights into the soil NO_x emission and its influences on atmospheric chemistry and composition. More studies in terms of soil NO_x emissions, particularly during springtime, are in need to validate and generalize our model results.

We should not ignore the uncertainties regarding the BDSNP scheme. The default 75/25 split in fertilizer application may be not widely suitable for the globe. Using a 20/80 split, as is commonly used in crop modeling (Jägermeyr et al., 2021), or a 40/60 split, as has been reported to be common in Northeast China (Zheng et al., 2023), would be expected to result in differences in the magnitude and timing of emissions compared to the default scheme. Among other impacts, there is no canopy interception of emitted soil NO_x at planting, which would result in substantially larger emissions to the atmosphere under the default 75/25 split than in a 20/80 split. In addition, because BDSNP applies the 25% topdressing application evenly over the growing season following the 75% basal application, it is less likely to produce sizable pulses of emissions. Because fertilizer applications are kept constant and global fertilizer emissions are constrained to 1.8 Tg N, the BDSNP mechanism is unable to reproduce historical trends or capture significant interannual variability in emissions.

The discrepancies between NO_2 and NH_3 column densities suggest substantial differences in the soil emission mechanisms of NO_x and NH_3, especially after fertilization. Future studies

could incorporate a dynamic bidirectional NH_3 scheme alongside the BDSNP scheme to further investigate the nature of fertilizer-induced emission pulses.

Data availability

The OMI satellite data are from the NASA Goddard Space Flight Center, Goddard Earth Sciences Data and Information Services Center (GES DISC) (https://disc.gsfc.nasa.gov/datasets/OMI_MINDS_NO2d_1.1/summary) and the IASI satellite observations are from the IASI Portal (https://iasi.aeris-data.fr/nh3_iasi_a_arch). The real-time hourly air pollutant measurements including NO_2, O_3, and $PM_{2.5}$ are released by Ministry of Ecology and Environment, China and can be accessed on the website https://quotsoft.net/air/. The MEIC Group and the EDGAR Team for the MEIC and HATP emission inventories which are available at http://www.meicmodel.org and https://edgar.jrc.ec.europa.eu/dataset_htap_v3, respectively.

Author contribution

TF and GL conceptualized the ideas, verified the conclusions, and revised the paper. TF conducted research, designed the experiments, carried out the methodology, performed the simulation, processed the data, prepared the data visualization, and prepared the paper, with contributions from all authors. SZ and NB provided the treatment of meteorological data, analyzed the study data, validated the model performance, and reviewed the paper. XL, YP, YS, and RW provided the observation data and emission inventories, and reviewed the paper. XT and LM provided critical reviews in the pre-publication stage.

Competing interests

The authors declare no conflicts of interest relevant to this study.

Acknowledgments

We thank the two anonymous reviewers for their insightful comments, which have greatly improved the quality of this paper. This work was supported by the National Natural Science Foundation of China (Grants 42371080 and 42371093), the Natural Science Foundation of Shaanxi Province (Grant 2017JM4023), the Natural Science Foundation of Ningbo Municipality (2023J208), and the Science and Technology Innovation 2025 Major Project of Ningbo Municipality (Grants 2022Z032, 2022Z189, and 2023Z139). This study was also sponsored by K. C. Wong Magna Fund in Ningbo University.

References

Almaraz, M., Bai, E., Wang, C., Trousdell, J., Conley, S., Faloona, I. and Houlton, B. Z.: Agriculture is a major source of NOx pollution in California, Sci Adv, 4(1), eaao3477, doi:10.1126/sciadv.aao3477, 2018.

Anderson, I. C. and Levine, J. S.: Simultaneous field measurements of biogenic emissions of nitric oxide and nitrous oxide, J Geophys Res, 92, 965–976, doi:10.1029/JD092iD01p00965, 1987.

Bauwens, M., Compernolle, S., Stavrakou, T., Müller, J. F., van Gent, J., Eskes, H., Levelt, P. F., van der A, R., Veefkind, J. P., Vlietinck, J., Yu, H. and Zehner, C.: Impact of Coronavirus Outbreak on NO_2 Pollution Assessed Using TROPOMI and OMI Observations, Geophys. Res. Lett., 47(1), e87978, doi:10.1029/2020GL087978, 2020.

Bennetzen, E. H., Smith, P. and Porter, J. R.: Decoupling of greenhouse gas emissions from global agricultural production: 1970-2050, Global Change Biol, 22(2), 763–781, doi:10.1111/gcb.13120, 2016.

Bouwman, A. F., Boumans, L. J. M. and Batjes, N. H.: Modeling global annual N_2O and NO emissions from fertilized fields, Global Biogeochem. Cycles, 16(4), 1080–28–9, doi:10.1029/2001GB001812, 2002.

Buchholz, R. R., Emmons, L. K., Tilmes, S. and The CESM Development Team: CESM2.1/CAM-chem Instantaneous Output for Boundary Conditions, UCARNCAR - Atmospheric Chemistry Observations and Modeling Laboratory, doi:10.5065/NMP7-EP60, 2019.

Cárdenas, L., Rondón, A., Johansson, C. and Sanhueza, E.: Effects of soil moisture, temperature, and inorganic nitrogen on nitric oxide emissions from acidic tropical savannah soils, J Geophys Res, 98(D8), 14783–14790, doi:10.1029/93JD01020, 1993.

Chen, F. and Dudhia, J.: Coupling an advanced land surface-hydrology model with the Penn State-NCAR MM5 modeling system. Part II: Preliminary model validation, Mon. Weather Rev., 129(4), 569–585, doi:10.1175/1520-0493(2001)129<0569:caalsh>2.0.co;2, 2001.

Chou, M.-D. and Suarez, M. J.: A solar radiation parameterization for atmospheric studies, edited by M. J. Suarez. 1999.

Chou, M.-D., Suarez, M. J., Liang, X.-Z. and Yan, M. M. H.: A thermal infrared radiation parameterization for atmospheric studies, edited by M. J. Suarez. 2001.

Clarisse, L., Franco, B., Van Damme, M., Di Gioacchino, T., Hadji-Lazaro, J., Whitburn, S., Noppen, L., Hurtmans, D., Clerbaux, C. and Coheur, P.: The IASI NH_3 version 4 product: averaging kernels and improved consistency, Atmos. Meas. Tech., 16(21), 5009–5028, doi:10.5194/amt-16-5009-2023, 2023.

Crippa, M., Guizzardi, D., Butler, T., Keating, T., Wu, R., Kaminski, J., Kuenen, J., Kurokawa, J., Chatani, S., Morikawa, T., Pouliot, G., Racine, J., Moran, M. D., Klimont, Z., Manseau, P. M., Mashayekhi, R., Henderson, B. H., Smith, S. J., Suchyta, H., Muntean, M., Solazzo, E., Banja, M., Schaaf, E., Pagani, F., Woo, J.-H., Kim, J., Monforti-Ferrario, F., Pisoni, E., Zhang, J., Niemi, D., Sassi, M., Ansari, T. and Foley, K.: The HTAP_v3 emission mosaic: merging regional and global monthly emissions (2000–2018) to support air quality modelling and policies, Earth System Science Data, 15(6), 2667–2694, doi:10.5194/essd-15-2667-2023, 2023.

Davidson, E. A.: Sources of nitric oxide and nitrous oxide following wetting of dry soil, Soil Science Society of America Journal, 56(1), 95–102, doi:10.2136/sssaj1992.03615995005600010015x, 1992.

Davidson, E. A., Potter, C. S., Schlesinger, P. and Klooster, S. A.: Model estimates of regional nitric oxide emissions from soils of the southeastern United States, Ecological Applications, 8(3), 748–759, doi:10.1890/1051-0761(1998)008[0748:MEORNO]2.0.CO;2, 1998.

Emmons, L. K., Schwantes, R. H., Orlando, J. J., Tyndall, G., Kinnison, D., Lamarque, J.-F., Marsh, D., Mills, M. J., Tilmes, S., Bardeen, C., Buchholz, R. R., Conley, A., Gettelman, A., Garcia, R., Simpson, I., Blake, D. R., Meinardi, S. and Pétron, G.: The Chemistry Mechanism in the Community Earth System Model Version 2 (CESM2), J. Adv. Model. Earth Syst., 12(4), e2019MS001882, doi:10.1029/2019MS001882, 2020.

Feng, T., Bei, N., Zhao, S., Wu, J., Li, X., Zhang, T., Cao, J., Zhou, W. and Li, G.: Wintertime nitrate formation during haze days in the Guanzhong basin, China: A case study,

693 Environ. Pollut., 243, 1057–1067, doi:10.1016/j.envpol.2018.09.069, 2018.

694 Feng, T., Zhao, S., Hu, B., Bei, N., Zhang, X., Wu, J., Li, X., Liu, L., Wang, R., Tie, X. and
695 Li, G.: Assessment of Atmospheric Oxidizing Capacity Over the Beijing-Tianjin-Hebei
696 (BTH) Area, China, J. Geophys. Res. Atmos., 126(7), e2020JD033834,
697 doi:10.1029/2020JD033834, 2021.

698 Feng, T., Zhao, S., Liu, L., Long, X., Gao, C. and Wu, N.: Nitrous acid emission from soil
699 bacteria and related environmental effect over the North China Plain, Chemosphere, 287,
700 132034, doi:10.1016/j.chemosphere.2021.132034, 2022.

701 Fu, X., Wang, T., Gao, J., Wang, P., Liu, Y., Wang, S., Zhao, B. and Xue, L.: Persistent
702 Heavy Winter Nitrate Pollution Driven by Increased Photochemical Oxidants in Northern
703 China, Environ. Sci. Technol., 54(7), 3881–3889, doi:10.1021/acs.est.9b07248, 2020.

704 Galbally, I. E. and Roy, C. R.: Loss of fixed nitrogen from soils by nitric oxide exhalation,
705 Nature, 275(5), 734–735, doi:10.1038/275734a0, 1978.

706 Gong, C., Wang, Y., Tian, H., Kou-Giesbrecht, S., Vuichard, N. and Zaehle, S.: Uncertainties
707 in fertilizer-induced emissions of soil nitrogen oxide and the associated impacts on ground-
708 level ozone and methane, EGUsphere, 1–17, doi:10.5194/egusphere-2025-1416, 2025.

709 Guenther, A., Karl, T., Harley, P., Wiedinmyer, C., Palmer, P. I. and Geron, C.: Estimates of
710 global terrestrial isoprene emissions using MEGAN (Model of Emissions of Gases and
711 Aerosols from Nature), Atmos. Chem. Phys., 6(11), 3181–3210, doi:10.5194/acp-6-3181-
712 2006, 2006.

713 Guo, L., Chen, J., Luo, D., Liu, S., Lee, H. J., Motallebi, N., Fong, A., Deng, J., Rasool, Q.
714 Z., Avise, J. C., Kuwayama, T., Croes, B. E. and FitzGibbon, M.: Assessment of Nitrogen
715 Oxide Emissions and San Joaquin Valley $PM_{2.5}$ Impacts From Soils in California, J.
716 Geophys. Res. Atmos., 125(24), e2020JD033304, doi:10.1029/2020JD033304, 2020.

717 Hall, S. J., Matson, P. A. and Roth, P. M.: NOx EMISSIONS FROM SOIL: Implications for
718 Air Quality Modeling in Agricultural Regions, Annu. Rev. Energy. Environ., 21(1), 311–346,
719 doi:10.1146/annurev.energy.21.1.311, 1996.

720 Hickman, J. E., Huang, Y., Wu, S., Diru, W., Groffman, P. M., Tully, K. L. and Palm, C. A.:
721 Nonlinear response of nitric oxide fluxes to fertilizer inputs and the impacts of agricultural
722 intensification on tropospheric ozone pollution in Kenya, Global Change Biol, 23(8), 3193–
723 3204, doi:10.1111/gcb.13644, 2017.

724 Hong, S. Y. and Lim, J.: The WRF single-moment 6-class microphysics scheme (WSM6),
725 Asia-Pac. J. Atmos. Sci., 42(2), 129–151, 2006.

726 Huang, L., Fang, J., Liao, J., Yarwood, G., Chen, H., Wang, Y. and Li, L.: Insights into soil

NO emissions and the contribution to surface ozone formation in China, Atmos. Chem. Phys., 23(23), 14919–14932, doi:10.5194/acp-23-14919-2023, 2023.

Huang, X., Song, Y., Li, M., Li, J., Huo, Q., Cai, X., Zhu, T., Hu, M. and Zhang, H.: A high-resolution ammonia emission inventory in China, Global Biogeochem. Cycles, 26(1), GB1030, doi:10.1029/2011GB004161, 2012.

Huang, Y., Hickman, J. E. and Wu, S.: Impacts of enhanced fertilizer applications on tropospheric ozone and crop damage over sub-Saharan Africa, Atmos. Environ., 180, 117–125, doi:10.1016/j.atmosenv.2018.02.040, 2018.

Huber, D. E., Steiner, A. L. and Kort, E. A.: Daily Cropland Soil NOx Emissions Identified by TROPOMI and SMAP, Geophys. Res. Lett., 47(2), e89949, doi:10.1029/2020GL089949, 2020.

Hudman, R. C., Moore, N. E., Mebust, A. K., Martin, R. V., Russell, A. R., Valin, L. C. and Cohen, R. C.: Steps towards a mechanistic model of global soil nitric oxide emissions: implementation and space based-constraints, Atmos. Chem. Phys., 12(1), 7779–7795, doi:10.5194/acp-12-7779-2012, 2012.

IPCC: Short-lived Climate Forcers, in Climate Change 2021 – The Physical Science Basis: Working Group I Contribution to the Sixth Assessment Report of the Intergovernmental Panel on Climate Change, pp. 817–922, Cambridge University Press, Cambridge. 2023.

Janjić, Z. I.: Nonsingular implementation of the Mellor–Yamada level 2.5 scheme in the NCEP Meso model. 2002.

Janssens-Maenhout, G., Crippa, M., Guizzardi, D., Dentener, F., Muntean, M., Pouliot, G., Keating, T., Zhang, Q., Kurokawa, J., Wankmüller, R., Denier van der Gon, H., Kuenen, J. J. P., Klimont, Z., Frost, G., Darras, S., Koffi, B. and Li, M.: HTAP-v2.2: A mosaic of regional and global emission grid maps for 2008 and 2010 to study hemispheric transport of air pollution, Atmos. Chem. Phys., 15(19), 11411–11432, doi:10.5194/acp-15-11411-2015, 2015.

Jägermeyr, J., Müller, C., Ruane, A. C., Elliott, J., Balkovic, J., Castillo, O., Faye, B., Foster, I., Folberth, C., Franke, J. A., Fuchs, K., Guarin, J. R., Heinke, J., Hoogenboom, G., Iizumi, T., Jain, A. K., Kelly, D., Khabarov, N., Lange, S., Lin, T.-S., Liu, W., Mialyk, O., Minoli, S., Moyer, E. J., Okada, M., Phillips, M., Porter, C., Rabin, S. S., Scheer, C., Schneider, J. M., Schyns, J. F., Skalsky, R., Smerald, A., Stella, T., Stephens, H., Webber, H., Zabel, F. and Rosenzweig, C.: Climate impacts on global agriculture emerge earlier in new generation of climate and crop models, Nature Food, 2(11), 873–885, 2021.

Kurokawa, J. and Ohara, T.: Long-term historical trends in air pollutant emissions in Asia: Regional Emission inventory in ASia (REAS) version 3, Atmos. Chem. Phys., 20(21), 12761–12793, doi:10.5194/acp-20-12761-2020, 2020.

Lamsal, L. N., Krotkov, N. A., Vasilkov, A., Marchenko, S., Qin, W., Yang, E.-S., Fasnacht, Z., Joiner, J., Choi, S., Haffner, D., Swartz, W. H., Fisher, B. and Bucsela, E.: Ozone Monitoring Instrument (OMI) Aura nitrogen dioxide standard product version 4.0 with improved surface and cloud treatments, Atmos. Meas. Tech., 14(1), 455–479, doi:10.5194/amt-14-455-2021, 2021.

Laville, P., Lehuger, S., Loubet, B., Chaumartin, F. and Cellier, P.: Effect of management, climate and soil conditions on N2O and NO emissions from an arable crop rotation using high temporal resolution measurements, Agr Forest Meteorol, 151(2), 228–240, doi:10.1016/j.agrformet.2010.10.008, 2011.

Li, G., Bei, N., Tie, X. and Molina, L. T.: Aerosol effects on the photochemistry in Mexico City during MCMA-2006/MILAGRO campaign, Atmos. Chem. Phys., 11(11), 5169–5182, doi:10.5194/acp-11-5169-2011, 2011a.

Li, G., Lei, W., Bei, N. and Molina, L. T.: Contribution of garbage burning to chloride and $PM_{2.5}$ in Mexico City, Atmos. Chem. Phys., 12(18), 8751–8761, doi:10.5194/acp-12-8751-2012, 2012.

Li, G., Lei, W., Zavala, M., Volkamer, R., Dusanter, S., Stevens, P. and Molina, L. T.: Impacts of HONO sources on the photochemistry in Mexico City during the MCMA-2006/MILAGO Campaign, Atmos. Chem. Phys., 10(14), 6551–6567, doi:10.5194/acp-10-6551-2010, 2010.

Li, G., Zavala, M., Lei, W., Tsimpidi, A. P., Karydis, V. A., Pandis, S. N., Canagaratna, M. R. and Molina, L. T.: Simulations of organic aerosol concentrations in Mexico City using the WRF-CHEM model during the MCMA-2006/MILAGRO campaign, Atmos. Chem. Phys., 11(8), 3789–3809, doi:10.5194/acp-11-3789-2011, 2011b.

Li, M., Liu, H., Geng, G., Hong, C., Liu, F., Song, Y., Tong, D., Zheng, B., Cui, H., Man, H., Zhang, Q. and He, K.: Anthropogenic emission inventories in China: A review, National Science Review, 4(6), 834–866, doi:10.1093/nsr/nwx150, 2017a.

Li, M., Zhang, Q., Kurokawa, J.-I., Woo, J.-H., He, K., Lu, Z., Ohara, T., Song, Y., Streets, D. G., Carmichael, G. R., Cheng, Y., Hong, C., Huo, H., Jiang, X., Kang, S., Liu, F., Su, H. and Zheng, B.: MIX: a mosaic Asian anthropogenic emission inventory under the international collaboration framework of the MICS-Asia and HTAP, Atmos. Chem. Phys., 17(2), 935–963, doi:10.5194/acp-17-935-2017, 2017b.

Li, T., Zhang, W., Yin, J., Chadwick, D., Norse, D., Lu, Y., Liu, X., Chen, X., Zhang, F., Powlson, D. and Dou, Z.: Enhanced-efficiency fertilizers are not a panacea for resolving the nitrogen problem, Global Change Biol, 24(2), e511–e521, doi:10.1111/gcb.13918, 2018.

Liu, C., Zheng, X., Zhou, Z., Han, S., Wang, Y., Wang, K., Liang, W., Li, M., Chen, D. and Yang, Z.: Nitrous oxide and nitric oxide emissions from an irrigated cotton field in Northern

799 China, Plant Soil, 332(1), 123–134, doi:10.1007/s11104-009-0278-5, 2010.

800 Liu, L., Wu, J., Liu, S., Li, X., Zhou, J., Feng, T., Qian, Y., Cao, J., Tie, X. and Li, G.:
801 Effects of organic coating on the nitrate formation by suppressing the N_2O_5 heterogeneous
802 hydrolysis: a case study during wintertime in Beijing–Tianjin–Hebei (BTH), Atmos. Chem.
803 Phys., 19(12), 8189–8207, doi:10.5194/acp-19-8189-2019, 2019.

804 Liu, X. J., Mosier, A. R., Halvorson, A. D. and Zhang, F. S.: Tillage and Nitrogen
805 Application Effects on Nitrous and Nitric Oxide Emissions from Irrigated Corn Fields, Plant
806 Soil, 276(1), 235–249, doi:10.1007/s11104-005-4894-4, 2005.

807 Liu, X., Ju, X., Zhang, F., Pan, J. and Christie, P.: Nitrogen dynamics and budgets in a winter
808 wheat–maize cropping system in the North China Plain, Field Crops Research, 83(2), 111–
809 124, doi:10.1016/S0378-4290(03)00068-6, 2003.

810 Liu, X., Zhang, Y., Han, W., Tang, A., Shen, J., Cui, Z., Vitousek, P., Erisman, J. W.,
811 Goulding, K., Christie, P., Fangmeier, A. and Zhang, F.: Enhanced nitrogen deposition over
812 China, Nature, 494(7438), 459–462, doi:10.1038/nature11917, 2013.

813 Lu, X., Ye, X., Zhou, M., Zhao, Y., Weng, H., Kong, H., Li, K., Gao, M., Zheng, B., Lin, J.,
814 Zhou, F., Zhang, Q., Wu, D., Zhang, L. and Zhang, Y.: The underappreciated role of
815 agricultural soil nitrogen oxide emissions in ozone pollution regulation in North China, Nat.
816 Commun., 12(1), 5021–9, doi:10.1038/s41467-021-25147-9, 2021.

817 Ma, R., Yu, K., Xiao, S., Liu, S., Ciais, P. and Zou, J.: Data-driven estimates of fertilizer-
818 induced soil NH_3, NO and N_2O emissions from croplands in China and their climate change
819 impacts, Global Change Biol, 28(3), 1008–1022, doi:10.1111/gcb.15975, 2022.

820 Matson, P. A., Naylor, R. and Ortiz-Monasterio, I.: Integration of Environmental,
821 Agronomic, and Economic Aspects of Fertilizer Management, Science, 280(5360), 112–115,
822 doi:10.1126/science.280.5360.112, 1998.

823 Murray, L. T., Jacob, D. J., Logan, J. A., Hudman, R. C. and Koshak, W. J.: Optimized
824 regional and interannual variability of lightning in a global chemical transport model
825 constrained by LIS/OTD satellite data, J. Geophys. Res. Atmos., 117(D), D20307,
826 doi:10.1029/2012JD017934, 2012.

827 Oikawa, P. Y., Ge, C., Wang, J., Eberwein, J. R., Liang, L. L., Allsman, L. A., Grantz, D. A.
828 and Jenerette, G. D.: Unusually high soil nitrogen oxide emissions influence air quality in a
829 high-temperature agricultural region, Nat. Commun., 6(1), 8753–10,
830 doi:10.1038/ncomms9753, 2015.

831 Potter, P., Ramankutty, N., Bennett, E. M. and Donner, S. D.: Characterizing the Spatial
832 Patterns of Global Fertilizer Application and Manure Production, Earth Interactions, 14, 1–
833 22, doi:10.1175/2009EI288.1, 2010.

Qiao, J., Wang, J., Zhao, D., Zhou, W., Schwenke, G., Yan, T. and De Li Liu: Optimizing N fertilizer rates sustained rice yields, improved N use efficiency, and decreased N losses via runoff from rice-wheat cropping systems, Agriculture, Ecosystems & Environment, 324, 107724, doi:10.1016/j.agee.2021.107724, 2022.

Seinfeld, J. H. and Pandis, S. N.: Atmospheric Chemistry and Physics - From Air Pollution to Climate Change, 2nd ed., John Wiley & Sons, New Jersey. 2006.

Sha, T., Ma, X., Zhang, H., Janechek, N., Wang, Y., Wang, Y., Castro García, L., Jenerette, G. D. and Wang, J.: Impacts of Soil NOx Emission on O_3 Air Quality in Rural California, Environ. Sci. Technol., 55(10), 7113–7122, doi:10.1021/acs.est.0c06834, 2021.

Shen, Y., Xiao, Z., Wang, Y., Xiao, W., Yao, L. and Zhou, C.: Impacts of Agricultural Soil NOx Emissions on O3 Over Mainland China, J. Geophys. Res. Atmos., 128(4), e2022JD037986, doi:https://doi.org/10.1029/2022JD037986, 2023.

Sillman, S.: The use of NOy , H2O2, and HNO3 as indicators for ozone-NOx-hydrocarbon sensitivity in urban locations, J. Geophys. Res. Atmos., 100(D7), 14175–14188, doi:10.1029/94JD02953, 1995.

Stehfest, E. and Bouwman, L.: N_2O and NO emission from agricultural fields and soils under natural vegetation: summarizing available measurement data and modeling of global annual emissions, Nutrient Cycling in Agroecosystems, 74(3), 207–228, doi:10.1007/s10705-006-9000-7, 2006.

Steinkamp, J. and Lawrence, M. G.: Improvement and evaluation of simulated global biogenic soil NO emissions in an AC-GCM, Atmos. Chem. Phys., 11(1), 6063–6082, doi:10.5194/acp-11-6063-2011, 2011.

Sun, X., Ritzema, H., Huang, X., Bai, X. and Hellegers, P.: Assessment of farmers' water and fertilizer practices and perceptions in the North China Plain, Irrigation and Drainage, 71(4), 980–996, doi:https://doi.org/10.1002/ird.2719, 2022.

Tan, W., Wang, H., Su, J., Sun, R., He, C., Lu, X., Lin, J., Xue, C., Wang, H., Liu, Y., Liu, L., Zhang, L., Wu, D., Mu, Y. and Fan, S.: Soil Emissions of Reactive Nitrogen Accelerate Summertime Surface Ozone Increases in the North China Plain, Environ. Sci. Technol., 57(34), 12782–12793, doi:10.1021/acs.est.3c01823, 2023.

Tang, K., Qin, M., Fang, W., Duan, J., Meng, F., Ye, K., Zhang, H., Xie, P., Liu, J., Liu, W., Feng, Y., Huang, Y. and Ni, T.: An automated dynamic chamber system for exchange flux measurement of reactive nitrogen oxides (HONO and NOx) in farmland ecosystems of the Huaihe River Basin, China, Sci. Total Environ., 745(C), 140867, doi:10.1016/j.scitotenv.2020.140867, 2020.

Tian, D., Zhang, Y., Mu, Y., Liu, J. and He, K.: Effect of N fertilizer types on N_2O and NO

emissions under drip fertigation from an agricultural field in the North China Plain, Sci. Total Environ., 715(C), 136903, doi:10.1016/j.scitotenv.2020.136903, 2020.

Tubiello, F. N., Salvatore, M., Rossi, S., Ferrara, A., Fitton, N. and Smith, P.: The FAOSTAT database of greenhouse gas emissions from agriculture, Environ. Res. Lett., 8(1), 015009, doi:10.1088/1748-9326/8/1/015009, 2013.

Vinken, G. C. M., Boersma, K. F., Maasakkers, J. D., Adon, M. and Martin, R. V.: Worldwide biogenic soil NOx emissions inferred from OMI NO_2 observations, Atmos. Chem. Phys., 14(1), 10363–10381, doi:10.5194/acp-14-10363-2014, 2014.

Vitousek, P. M., Naylor, R., Crews, T., David, M. B., Drinkwater, L. E., Holland, E., Johnes, P. J., Katzenberger, J., Martinelli, L. A., Matson, P. A., Nziguheba, G., Ojima, D., Palm, C. A., Robertson, G. P., Sanchez, P. A., Townsend, A. R. and Zhang, F. S.: Nutrient Imbalances in Agricultural Development, Science, 324, 1519–1520, doi:10.1126/science.1170261, 2009.

Wang, R., Bei, N., Wu, J., Li, X., Liu, S., Yu, J., Jiang, Q., Tie, X. and Li, G.: Cropland nitrogen dioxide emissions and effects on the ozone pollution in the North China plain, Environ. Pollut., 294, 118617, doi:10.1016/j.envpol.2021.118617, 2022a.

Wang, Y., Yao, Z., Zheng, X., Subramaniam, L. and Butterbach-Bahl, K.: A synthesis of nitric oxide emissions across global fertilized croplands from crop-specific emission factors, Global Change Biol, 28(14), 4395–4408, doi:10.1111/gcb.16193, 2022b.

Wen, L., Xue, L., Wang, X., Xu, C., Chen, T., Yang, L., Wang, T., Zhang, Q. and Wang, W.: Summertime fine particulate nitrate pollution in the North China Plain: increasing trends, formation mechanisms and implications for control policy, Atmos. Chem. Phys., 18(15), 11261–11275, doi:10.5194/acp-18-11261-2018, 2018.

Wu, J., Bei, N., Hu, B., Liu, S., Wang, Y., Shen, Z., Li, X., Liu, L., Wang, R., Liu, Z., Cao, J., Tie, X., Molina, L. T. and Li, G.: Aerosol–photolysis interaction reduces particulate matter during wintertime haze events, Proc. Natl. Acad. Sci. U.S.A., 117(18), 9755–9761, doi:10.1073/pnas.1916775117, 2020.

YAN, X., JIN, J.-Y., He, P. and LIANG, M.-Z.: Recent Advances on the Technologies to Increase Fertilizer Use Efficiency, Agricultural Sciences in China, 7(4), 469–479, doi:10.1016/S1671-2927(08)60091-7, 2008.

Yan, X., Ohara, T. and Akimoto, H.: Statistical modeling of global soil NOx emissions, Global Biogeochem. Cycles, 19(3), GB3019, doi:10.1029/2004GB002276, 2005.

Yienger, J. J. and Levy, H.: Empirical model of global soil-biogenic NOx emissions, J. Geophys. Res. Atmos., 100(D), 11447–11464, doi:10.1029/95JD00370, 1995.

Yu, Z., Liu, J. and Kattel, G.: Historical nitrogen fertilizer use in China from 1952 to 2018,

Earth System Science Data, 14(11), 5179–5194, doi:10.5194/essd-14-5179-2022, 2022.

Zhang, Q., Streets, D. G. and Carmichael, G. R.: Asian emissions in 2006 for the NASA INTEX-B mission, Atmos. Chem. Phys., 9(14), 5131–5153, doi:10.5194/acp-9-5131-2009, 2009.

Zhang, R., Wang, G., Guo, S., Zamora, M. L., Ying, Q., Lin, Y., Wang, W., Hu, M. and Wang, Y.: Formation of urban fine particulate matter, Chem. Rev., 115(10), 3803–3855, doi:10.1021/acs.chemrev.5b00067, 2015.

Zhang, Y., Liu, J., Mu, Y., Pei, S., Lun, X. and Chai, F.: Emissions of nitrous oxide, nitrogen oxides and ammonia from a maize field in the North China Plain, Atmos. Environ., 45(17), 2956–2961, doi:10.1016/j.atmosenv.2010.10.052, 2011.

Zhao, M., Tian, Y., Zhang, M., Yao, Y., Ao, Y., Bin Yin and Zhu, Z.: Nonlinear response of nitric oxide emissions to a nitrogen application gradient: A case study during the wheat season in a Chinese rice-wheat rotation system, Atmos. Environ., 102(C), 200–208, doi:10.1016/j.atmosenv.2014.11.052, 2015.

Zhao, R.-F., Chen, X.-P., Zhang, F.-S., Zhang, H., Schroder, J. and Römheld, V.: Fertilization and Nitrogen Balance in a Wheat–Maize Rotation System in North China, Agron. J., 98(4), 938–945, doi:10.2134/agronj2005.0157, 2006.

Zheng, Y., Ji, J. and Liu, S.: Effect of topdressing time on spring maize yield and nitrogen utilization in black soil of northeast China, Sci. Rep., 13(1), 11841–10, doi:10.1038/s41598-023-38724-3, 2023.

Zhu, Z., Stewart, B. A. and Fu, X.: Double cropping wheat and corn in a sub-humid region of China, Field Crops Research, 36(3), 175–183, doi:10.1016/0378-4290(94)90109-0, 1994.